Benefits of Selecting PMASR Machines as Traction Motors in Battery Electric Forklift Trucks

Matteo Olivo; Alberto Tessarolo
Dept. of Engineering and Architecture
University of Trieste
Trieste, Italy
e-mail: matteo.olivo@units.it;

Luca De Carli; Riccardo Pozzo
Electric Vehicle Driveline Division
PMP Industries Group
Coseano (UD), Italy

***Abstract*—The advantages of using PM-assisted synchronous reluctance motors as traction devices for electric forklift vehicles are investigated in this paper. Motor energy consumption and drive overall performance are analytically estimated through a simulation of a standard VDI-based driving cycle and compared with the corresponding results from a reference system driven using induction motors.**

Keywords—electric vehicles, traction motors, energy efficiency, brushless machines, industry applications.

I. INTRODUCTION

Forklifts and similar trucks for material handling represent the vast majority of off-road vehicles, being practically used in any industry in the world. Battery-Electric Forklift Trucks (BEFT) are generally preferred to Internal-Combustion Engine (ICE)-powered ones for indoor applications and their popularity is foreseen to increase, driven by the actual trends on transportation electrification [1].

Many academic and industrial researches on forklift-related topics can be found in the literature, involving any part of these vehicles such as batteries [2], traction and auxiliary motors [3]-[5], power electronics [6] and their overall management [7]. Particular focus needs to be placed on the optimal design of these systems and the maximization of their efficiency and energy saving, in order to achieve the best performance for battery vehicles. Since most of the truck power consumption is related to its movement, the traction motor(s) efficiency improvement is a key task to fulfil this kind of requirement.

Induction motors (IMs) have become the standard traction devices for electric forklifts, replacing the previous systems based on DC motors [8] thanks to their simplicity and relatively low cost (in terms of both manufacturing and maintenance). The main drawbacks related to IMs usage as traction motors is their relatively low torque density and limited efficiency [9]; for these reasons many industrial applications adopt Permanent Magnet Motors (PMMs) to meet their tight requirements in terms of compactness and energy consumption [10].

Among all the topologies of PMMs, Interior Permanent Magnet (IPM) machines are preferred for traction applications because they guarantee a wider speed operating range compared to Surface Permanent Magnet (SPM) machines [11]. Another valid choice for this kind of applications is Synchronous-Reluctance (SynRel) machines, which do not require PMs for torque generation, thus they have a more competitive cost compared to IPM motors, although they cannot withstand the extremely advantageous torque density that the latter usually yield [12]. For these reasons PM-Assisted Synchronous-Reluctance (PMASR) motors have gained great popularity as traction devices, representing the right trade-off between the two mentioned machines strengths since they provide a superior torque density compared to SynRel machines with a limited manufacturing cost thanks to the reduced PMs volume.

Compared to IMs, drawbacks of PMASR machines that limit their usage as forklift trucks traction motors are their higher control complexity [14], their larger cost [15] and some fault-tolerance related issues [16], but they are gaining popularity thanks to the strong efforts of academic and industrial researchers [17]-[23]. This paper tries to contribute to this field by comparing the energy consumption of a BEFT IM-based traction system and a PMASR-based one, according to a standard working cycle. More in detail, the traction-related prescriptions of the testing cycle as per VDI 2198 guideline [24] have been applied to two different traction systems designed for a 3.5 t/7000 lbs BEFT to compare the battery energy/charge consumption per standard cycle and the overall performance of the two machine-systems.

The paper is organized as follows. Section II presents an overview on BEFT traction system and the main characteristics of the two electrical machines being studied. It also briefly presents the standard reference testing cycle to be used in the following. Section III provides the theoretical background for the kinematic model for computing the motor energy consumption needed to complete the reference working cycle. The results of the performed calculations are presented and discussed in Section IV, finally leading to the conclusions drawn in Section V.

II. FORKLIFT TRUCK TRACTION SYSTEM

The typical traction system for a BEFT is shown in Fig. 1. It is composed of two semi-independently driven motor-

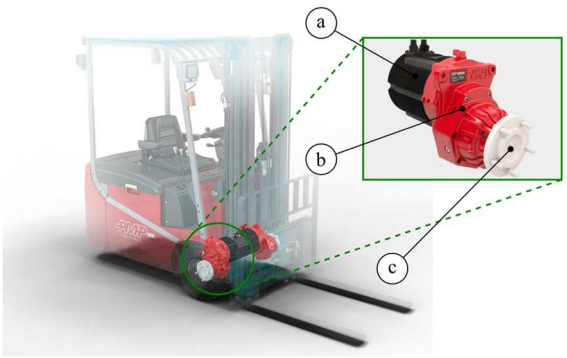

Fig. 1 BEFT traction system (courtesy of PMP Industries Group) (a) Electric motor + inverter (b) Gearbox (c) Truck wheel hub.

gearbox-wheel systems mounted on the truck front axle. The gearbox is generally a two-stage system having an overall speed reduction ratio (RR) in the range of 20/40:1, depending on the forklift-truck ratings and specifications. The first stage is a parallel-shaft gearbox driven by the "fast" shaft mechanically integrated with the electric motor; the output stage is a planetary gearbox with its planetary carrier directly attached to the truck wheel hub.

Each motor is controlled by a PWM inverter with its DC stage connected to the truck main battery, generally having a rated voltage of 48 or 80 V. The inverter is capable of four-quadrant operation to allow for truck regenerative braking and forward-backward running.

The nameplate data of two reference machines (IM vs PMASR) are collected in Table I. It can be noticed how the two machines have comparable size and ratings, but the PMASR motor features a +40% torque-per-mass density with respect to the IM.

TABLE I
NAMEPLATE DATA AND GENERAL CHARACTERISTICS OF REFERENCE TRACTION MACHINES.

Quantity		IM	PMASR
Size (out- diameter × length)	[mm]	240×110	
Battery voltage	[V]	80	
Rated current (line, RMS)	[A]	129	150
Rated power	[kW]	9	12
Base frequency	[Hz]	68	100
Number of poles	[-]	4	6
Rated torque	[Nm]	43.0	57.3
Torque density	[Nm/dm^3]	16.3	21.7
	[Nm/kg]	1.34	1.88
Mass	[kg]	32.0	30.4
Duty type		S2 – 60 min	
Thermal class		H (180°C)	

A. Reference power-consumption testing cycle

The standard driving cycle as per VDI 2198 (hereinafter referred to as VDI cycle) is taken as reference by international standards such as ISO 23308-1 for the energy efficiency rating on industrial vehicles [25]. It consists of a standard sequence of actions involving all the functional components of the forklift trucks, i.e., it is not specifically focused on the traction system but involves, for instance, the lifting mechanism as well. Each cycle sub-operation is characterized by specific parameters such as travelled distance, speed conditions, truck load and movement direction.

Since this paper is focused on the performance comparison of traction motors, a simplified driving cycle based on the VDI one has been defined. This cycle takes just the prescribed traction-related operations from the standard VDI cycle, with the same specifications. Furthermore a few simplifications and assumptions has been made to obtain a suitable sequence of operations that can be easily implemented through the theoretical model described in Section III:

- Since the forward/backward movement is realized by simply reverting the motor phase sequencing, this prescription from standard VDI cycle can be ignored and the actual inverter four-quadrant operation is limited to a two-quadrant one (motoring/braking).
- Each VDI cycle phase is subdivided into different subphases of three kinds: acceleration, constant speed (curving), braking.
- The truck maximum speed at the end of an acceleration phase is set equal to v_{max} = 4.15 m/s (≈15 km/h); besides the constant speed at each curve is denoted as v_{min} and it is equal to 0.25 m/s (0.9 km/h) as per standard VDI cycle prescription.

The simplified driving cycle is reported in Table II, detailing the information required to implement the kinetic model described in the next section. The abbreviations used in Table II are the following: U = truck unloaded, L = truck at full load, A = acceleration, B = braking, C = curving at constant speed.

TABLE II
REFERENCE DRIVING CYCLE.

VDI phase	Sub-phase	Loading status	Type	Distance travelled	Speed diagram
1	1.1	U	A	≈25 m	$0 \rightarrow v\ (\leq v_{max})$
	1.2		B	≈5 m	$v \rightarrow v_{min}$
	1.3		C	3.14 m	v_{min}
	1.4		B	0.1 m	$v_{min} \rightarrow 0$
	1.5		A	≈0.8 m	$0 \rightarrow v$
	1.6		B	≈0.7 m	$v \rightarrow 0$
	Phase 1 total			**≈35 m**	**-**
2	2.1	L	A	≈0.8 m	$0 \rightarrow v$
	2.2		B	≈0.7 m	$v \rightarrow 0$
	2.3		A	0.1 m	$0 \rightarrow v_{min}$
	2.4		C	3.14 m	v_{min}
	2.5		B	0.4 m	$v_{min} \rightarrow 0$
	Phase 2 total			**≈5 m**	-
3	3.1	L	A	≈25 m	$0 \rightarrow v\ (\leq v_{max})$
	3.2		B	≈5 m	$v \rightarrow v_{min}$
	3.3		C	3.14 m	v_{min}
	3.4		B	0.4 m	$v_{min} \rightarrow 0$
	3.5		A	≈0.8 m	$0 \rightarrow v$
	3.6		B	≈0.7 m	$v \rightarrow 0$
	Phase 3 total			**≈35 m**	**-**
4	4.1	U	A	≈0.8 m	$0 \rightarrow v$
	4.2		B	≈0.7 m	$v \rightarrow 0$
	4.3		A	0.2 m	$0 \rightarrow v_{min}$
	4.4		C	3.14 m	v_{min}
	4.5		B	0.1 m	$v_{min} \rightarrow 0$
	Phase 4 total			**≈5 m**	**-**
Driving cycle total				**≈80 m**	**-**

III. ANALYTICAL MODEL FOR ELECTRIC CONSUMPTION CALCULATION

The energy consumption per reference driving cycle can be calculated according to the traction machine characteristic curves, i.e., the maps that correlate the motor current, voltage and efficiency to the current torque and speed. The latter are, in turn, determined from the kinetic state of the vehicle during the driving cycle in Table II. It is worth defining the current, voltage and efficiency characteristic in the form of torque and speed Look-Up Tables (LUTs); this is done by means of a proper set of Finite-Element Analysis (FEAs) on the reference machine geometries, both working as motors and generators (brakes).

This section collects the theoretical relationships that lead to compute the motor torque and speed from the actual car position and speed in the reference driving cycle. More in detail subsection III.A recalls the main relationships for the

truck/motor mechanical dynamics, whereas section III.B presents a model for the feed-forward motor speed control; in fact, since we are interested in the evaluation of the motor consumption and it is assumed that the motor driving system losses are quite negligible compared to the traction machine power, we can ignore the actual feedback control dynamics and adopt a simpler model where the motor performance is inferred from the present truck speed and position, by calculating the acceleration required to reach the target kinetic state at the end of each sub-phase.

A. *Truck and motor dynamics*

At first it is worth writing the relationship between the motor speed n (in rpm) and the truck speed v:

$$n = \frac{30}{\pi}\frac{R}{r_w} v = K_{rpm} v \tag{1}$$

where R is the total gearbox speed reduction ratio, r_w is the truck wheel radius and the speed-to-rpm gain $K_{rpm}=30/\pi\ R/r_w$ has been introduced for the sake of convenience. Similarly, the truck acceleration a is related to the net driving torque T as per the following equation:

$$a = \frac{R}{\lambda\, m\, r_w} T = \frac{K_{acc}}{\lambda} T \tag{2}$$

being m the full driven mass (i.e. the truck mass at rated load per motorized wheel), λ the load factor (i.e. the current truck mass with respect to full load mass) and the rated acceleration gain $K_{acc} = R/(m\ r_w)$. Since the reference driving cycle considers only the truck at full load or at no load, then the actual load factor can either be 1 at full load or $\lambda_0 = M_0/M$ at no-load (where M_0 denotes the truck mass at no load and M is the same at full load). It is worth noticing that the sign of the acceleration in (2) is the same as the for net torque, i.e., if the latter is positive the truck is accelerating, whereas if it is negative it is decelerating.

The net driving torque is given by subtracting the friction (always braking) torque on motor side T_{brk} and the motor inertial contribute from the current motor torque T_m:

$$T = T_m - T_{brk} - \frac{\pi}{30} J \dot{n} \tag{3}$$

where $\dot{n}$ is the motor speed time-derivative (i.e., the angular acceleration) and $J = J_m + J_w/R^2$ is the total driven-shaft inertia, computed from the motor and wheel moment of inertia, which are respectively J_m and J_w. The breaking torque can be assumed as a function of the motor speed, which is directly related to the vehicle speed as per (1); in this paper the braking torque has been estimated from some field data according to the following procedure.

The speed and current recordings of the traction motors mounted on a reference truck have been used to calculate the motor torque (by reverting the machine characteristic current LUT), the vehicle acceleration and, thus, the driveshaft angular acceleration during the vehicle operation; from this data the experimental breaking torque was obtained combining (2) and (3), i.e.:

$$T_{brk,exp} = T_{m,exp} - \frac{\pi}{30} J \dot{n}_{exp} - \frac{\lambda\, a_{exp}}{K_{acc}} \tag{4}$$

where the subscript "exp" has been added to highlight that these values come from experimental readings. From this data the friction factor has been calculated:

$$B_{exp} = \frac{T_{brk,exp}}{n_{exp}} \tag{5}$$

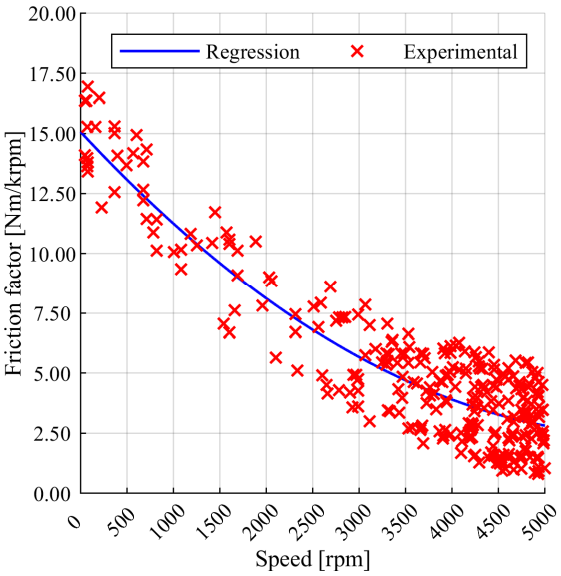

Fig. 2 Regression of friction factor from experimental data.

and then a quadratic regression function $\tilde{B}(n)$ has been defined accordingly. The regression function and the experimentally determined friction factor values are plotted in Fig. 2; the regression model allows one to compute the truck friction torque in the following as:

$$T_{brk} = \tilde{B}(n)\, n \tag{6}$$

B. *Feed-forward control model*

As mentioned above, a simple control model can be implemented to simulate the actual truck drifting during the driving cycle. The basic idea is, given the present truck position and speed, determining the acceleration required to get to the target kinetic state at the end of the current subphase. From the acceleration the required motor target torque is then determined and if the latter is compatible with the motor rating, then its working point is calculated, otherwise the target torque requirement is lowered to the maximum feasible torque value.

To determine the target acceleration, we start by writing down the car kinematic equations that give the target kinetic state (p_{obj}, v_{obj}) from the current one (p, v):

$$\begin{cases} p_{obj} = p + v\,\Delta t + \frac{1}{2} a_{obj}\,\Delta t^2 \\ v_{obj} = v + a_{obj}\,\Delta t \end{cases} \tag{7}$$

being p the truck position, v its velocity, a its acceleration and Δt the time required to complete the current subphase from the present position. Manipulating this expression, the target acceleration is obtained:

$$a_{obj} = \frac{v_{obj}^2 - v^2}{2\left(p_{obj} - p\right)} \tag{8}$$

The acceleration calculated as per (8) may result in an excessive value, so its magnitude is limited to the prescriptions as per [26] to maintain an adequate level of comfort for the truck driver.

From the target acceleration the corresponding target motor torque is calculated by manipulating (2) and (3):

$$T_{m,obj} = \frac{\lambda}{K_{acc}} a_{obj} + T_{brk} + \frac{\pi}{30} J \dot{n} \tag{9}$$

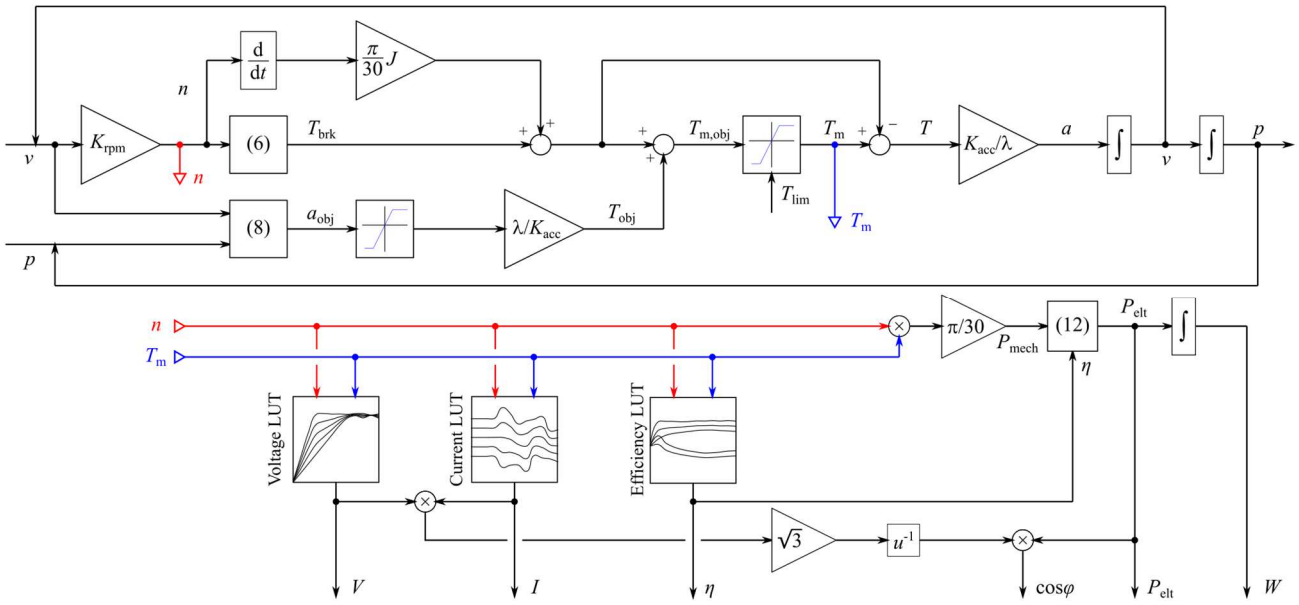

Fig. 3 Workflow for the analytical calculation of vehicle dynamics and motor performance during the reference driving cycle.

with T_{brk} calculated as per (6). The actual motor torque magnitude is determined by taking the least between the target value as per (9) and the maximum torque allowed at the present motor speed that is compatible with the voltage and current limits.

Once the motor torque is determined then the actual acceleration is computed trough (3) and (2); the corresponding truck speed and position can be then easily determined by integration. If a discrete time-system is considered it can be written as:

$$\begin{aligned} v_{k+1} &= v_k + a_k\ \tau_s \\ p_{k+1} &= p_k + v_k\ \tau_s \end{aligned} \tag{10}$$

being p_k, v_k and a_k the position, speed and acceleration at the k-th time-sample, with sampling time equal to τ_s.

The motor performance is finally calculated from the voltage, current and efficiency LUTs at the corresponding machine torque and speed working point; these lead to compute the remaining variables such as the mechanical power P_{mech}, the electric (active) power P_{elt}, the power factor cosφ and the battery energy consumption W:

$$P_{mech} = \frac{\pi}{30} T_m\ n \tag{11}$$

$$P_{elt} = \begin{cases} P_{mech}/\eta, & \text{if } T_m > 0 \\ P_{mech}\ \eta, & \text{if } T_m < 0 \end{cases} \tag{12}$$

$$\cos\varphi = \frac{P_{elt}}{\sqrt{3}\ V(T_m, n)\ I(T_m, n)} \tag{13}$$

$$W_k = \sum_{i=1}^{k} P_{elt,i}\ \tau_s \tag{14}$$

where $V(T_m,n)$, $I(T_m,n)$ and $\eta(T_m,n)$ are respectively the motor voltage, current and efficiency at the present torque and speed, calculated from the determined LUTs and W_k denotes the energy at k-th time-sample. Assuming that the battery voltage V_{DC} remains unchanged during the driving cycle, the charge consumption is simply given by W/V_{DC}.

Fig. 3 summarizes the whole vehicle dynamics and traction control workflow scheme. The main data required to perform the driving cycle simulation are collected in Table III.

TABLE III
REFERENCE TRUCK PARAMETERS.

Quantity	Symbol	Value
Gearbox speed reduction ratio	R	31.04
Wheel radius	r_w	290 mm
Truck full-load mass	M	9210 kg
Truck no-load mass	M_0	5710 kg
Nr. of motorized wheels	N_w	2
Motor moment of inertia (IM)	J_m	0.037 kg m^2
Motor moment of inertia (PMASR)		0.028 kg m^2
Wheel moment of inertia	J_w	0.850 kg m^2
Acceleration limit (acceleration)	a_{lim}	1.8 m/s^2
Acceleration limit (braking)		–2.2 m/s^2
Current RMS limit	I_{lim}	250 A
Sampling time	τ_s	10 ms

IV. RESULTS

The reference driving cycle presented in section II.A is applied to the truck traction system following the procedure presented in section III, considering the two reference motors given by Table I and the reference truck parameters shown in Table III. The results obtained from the two simulations are presented and discussed in this section.

First it is worth verifying that whichever machine is chosen the overall BEFT dynamics remains unchanged i.e., the vehicle completes the reference driving cycle in a comparable amount of time and following similar position and speed profiles. This verification is graphically shown in Fig. 4, where the truck position and speed vs. time are plotted for the two traction systems being studied (i.e., the IM-based and the PMASR-based one). It can be noticed how both the corresponding position and speed profile are practically overlapping, so the overall vehicle dynamics is the same for the two traction systems being studied; thus, the motor performance comparison made in the following is correct and homogeneous. It can be also noticed that phase 1 of the driving cycle (truck unloaded) is completed in 31.4 s, phases 2-3

(truck at full load) are completed in 49 s and finally phase 4 (truck unloaded) is completed in 18.2 s, giving a total driving cycle duration of 98.6 s, with roughly the same completion time for the unloaded or loaded phase. Figures from Fig. 5 to Fig. 8 show the comparison between some of the motor quantities for each traction system being plotted vs. the truck position during the driving cycle. Each plot shows the truck speed vs. its position as well, to help identify the present driving cycle sub-phase.

If the traction machine current and power factor (PF) are considered (shown, respectively, in Fig. 5 and Fig. 6) it can be noticed how the IM current absorption is slightly more than that of the PMASR machine (especially in the two 25 m-long acceleration phases, where most of the motor torque is required) but the actual active current (i.e. its torque-producing quota) for the IM is less than in the corresponding PMASR case, since the latter presents a PF close to 1 for the whole operation, whereas the former features a PF always below the value of 0.9. The IM working PF is even worse in the braking phases (which can be observed in Fig. 5 at the points where the current absorption becomes negative i.e., the motor is actually working as a generator); in fact the IM functioning as a generator requires a strong amount of magnetizing (reactive) current from the inverter supply to work properly [27]. Other phases where the IM current/PF performance is relatively poor if compared to PMASR are the constant-speed ones (i.e., sub-phases 1.3, 2.4, 3.3, 4.4). This is caused by the fact that during this operation the motor operate at very low speed and torque thus, again, the IM magnetizing current becomes particularly disadvantageous if compared to the total one. This difference is especially important in many practical BEFT scenarios, where the truck is required to perform several start-and-stop operations with relatively low speed and travelled distance.

Fig. 7 compares the machine energy conversion efficiency for the two traction-systems being studied. As expected, the PMASR machine has a superior efficiency since it has no rotor losses, whereas the IM efficiency is particularly poor in the regenerative braking phase, since the high magnetizing current causes large stator winding losses.

The considerations about active current and efficiency for the two machines are well summarized in Fig. 8, where the net battery energy consumption is shown (taking regenerative breaking into account). It can be noticed how the IM energy flow is particularly diverging from the PMASR one, especially in the full-load "long" acceleration phase (i.e., sub-phase 3.1) and in the constant-speed operation. The overall traction-related energy consumption per driving cycle for the

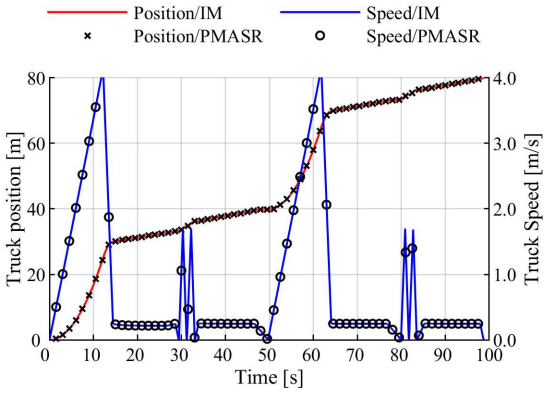

Fig. 4 Comparison of truck kinetic state during the reference driving cycle.

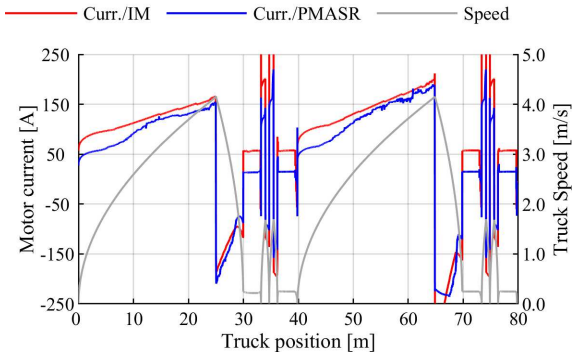

Fig. 5 Comparison of the motor current consumption in the reference driving cycle.

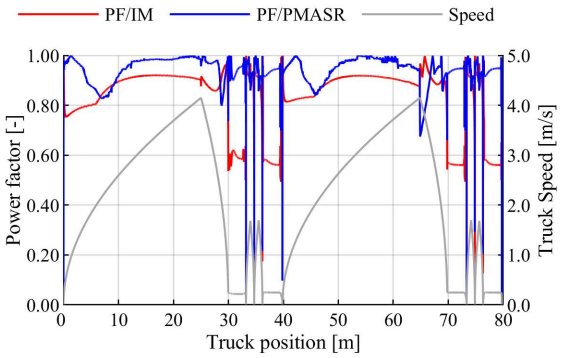

Fig. 6 Comparison of the motor power factor in the reference driving cycle.

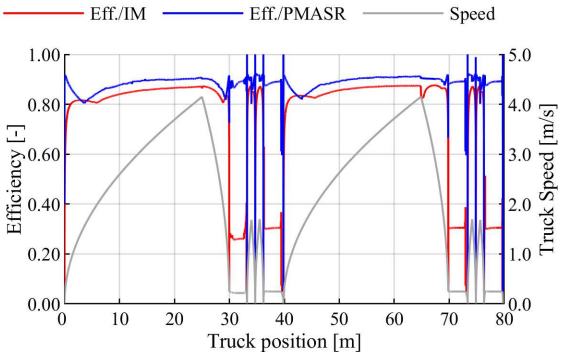

Fig. 7 Comparison of the motor efficiency in the reference driving cycle.

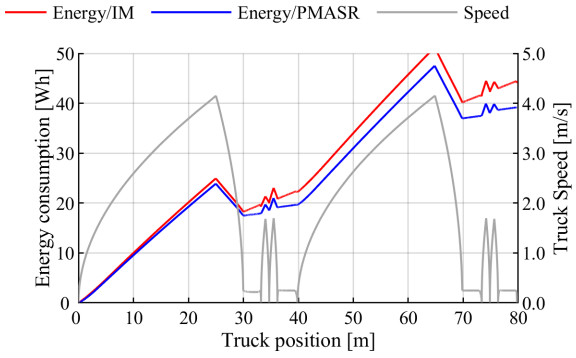

Fig. 8 Comparison of the battery energy consumption in the reference driving cycle.

IM-driven BEFT is roughly 44 Wh (158.4 kJ) that lowers to 40 Wh (144 kJ) if the PMASR-based system is considered, with approximately 10% of energy saving.

In order to convert this comparison into real-life experience, the simulation data can be used to estimate the battery discharge time in working conditions, i.e., the battery duration extension in a working cycle. Let us suppose that each BEFT mounts a standard battery with total full-charged energy of 36 kWh; it can also be assumed that the overall non-traction related energy consumption in a std. VDI cycle is ≈80% of the overall traction energy consumption (i.e., twice the motor consumption here calculated, since the truck is equipped with two traction motors, according to Table III). Furthermore, experience has shown that the standard VDI cycle is much demanding if compared to everyday forklift operation, so a 60% reduction factor is considered. With all these assumptions the total number of "real" working cycles that a BEFT can complete with a full battery charge is ≈380 with the IM-based traction or ≈420 if the PMASR case is considered. Thus, assuming an overall duration of 120 s per cycle the energy provided by the truck battery is enough for ≈12.5 hours of operation with IM-powered BEFT or equivalently ≈14 hours with the PMASR-based one.

V. Conclusions

In this paper the traction energy consumption of a BEFT during a standard-based driving cycle has been investigated. Two different scenarios have been considered, i.e., a reference IM-driven vehicle and a novel type implementing a pair of PMASR motors as traction devices. Given the two machine performance models, a simple approach based on the vehicle dynamics has been implemented and used to compute the overall energy consumption during a quasi-VDI test driving cycle.

The calculations have demonstrated how the use of a PM-based traction drive allows for an overall energy saving in the order of 10% if compared to usual IM-driven trucks. The PMASR traction is shown to be particularly advantageous in terms of active current and efficiency for regenerative braking and low-speed operation.

References

[1] J. Li, G. Lutzemberger, D. Poli, C. Scarpelli and T. Piazza, "Simulation and experimental validation of a hybrid forklift truck," 2019 AEIT International Conference of Electrical and Electronic Technologies for Automotive (AEIT AUTOMOTIVE), 2019, pp. 1-6

[2] M. Jiao, F. Pan, X. Huang and X. Yuan, "Application potential of second-life lithium-ion battery on forklift," 2021 IEEE 4th International Electrical and Energy Conference (CIEEC), 2021, pp. 1-5

[3] M. V. Terzic, B. Bilgin and A. Emadi, "Switched Reluctance Motor Design for a Forklift Traction Application," 2018 XIII International Conference on Electrical Machines (ICEM), 2018, pp. 812-818.

[4] T. A. Minav, L. I. E. Laurila and J. J. Pyrhönen, "Effect of driving electric machine type on the system efficiency of an industrial forklift," 2012 XXth International Conference on Electrical Machines, 2012, pp. 1964-1970.

[5] C. T. P. Nguyen, J. P. F. Trovao, B. -H. Nguyen and M. C. Ta, "Powertrain Analysis of an All-Wheel-Drive Off-Road Electric Vehicle," 2019 IEEE Vehicle Power and Propulsion Conference (VPPC), 2019, pp. 1-6.

[6] F. Crescimbini, V. Serrao and L. Solero, "Power Electronics Building Block (PEBB) for Static Conversion Apparatus Devoted to Low-Voltage Fed Electric Drives," 2005 IEEE 36th Power Electronics Specialists Conference, 2005, pp. 772-778.

[7] S. D. V. R. Vadlamudi, V. Kumtepeli, S. Ozcira and A. Tripathi, "Hybrid energy storage power allocation and motor control for electric forklifts," 2016 Asian Conference on Energy, Power and Transportation Electrification (ACEPT), 2016, pp. 1-5.

[8] N. C. Park, J. H. Kim, H. S. Mok and S. H. Kim, "Development of operation algorithm for 2.5 ton electric forklift using induction motors," 2007 7th Internatonal Conference on Power Electronics, 2007, pp. 283-288.

[9] H. B. Ertan, M. S. Siddique, S. Koushan and B. J. Azuaje-Berbecí, "Designing High Power Density Induction Motors for Electric Propulsion," 2022 IEEE 20th International Power Electronics and Motion Control Conference (PEMC), 2022, pp. 553-558.

[10] C. -T. Liu et al., "Cost-Effective Assessment of Surface-Mounted Permanent-Magnet Motors for Refrigerant Compressor Applications Used in High-Temperature Environments," in IEEE Transactions on Industry Applications, vol. 58, no. 4, pp. 5503-5509, July-Aug. 2022.

[11] B. Ge, M. Liu, J. Dong and W. Liu, "Torque Production Limit of Surface Permanent Magnet Synchronous Machines and Their Electromagnetic Scalability," in IEEE Transactions on Industry Applications, vol. 57, no. 5, pp. 4353-4362, Sept.-Oct. 2021.

[12] M. Chowdhury, M. Islam and I. Husain, "Synchronous Reluctance Machines for Low Torque Ripple Requiring Applications," 2022 IEEE Energy Conversion Congress and Exposition (ECCE), 2022, pp. 1-8.

[13] M. Oh and I. Husain, "Optimal Torque Distribution of Dual-Motor All-Wheel Drive Electric Vehicles for Maximizing Motor Energy Efficiency," 2021 IEEE Transportation Electrification Conference & Expo (ITEC), 2021, pp. 188-193.

[14] D. Pasqualotto, S. Rigon and M. Zigliotto, "Sensorless Speed Control of Synchronous Reluctance Motor Drives Based on Extended Kalman Filter and Neural Magnetic Model," in IEEE Transactions on Industrial Electronics, vol. 70, no. 2, pp. 1321-1330, Feb. 2023.

[15] A. M. Bazzi and P. T. Krein, "Comparative evaluation of machines for electric and hybrid vehicles based on dynamic operation and loss minimization," 2010 IEEE Energy Conversion Congress and Exposition, 2010, pp. 3345-3351.

[16] B. Wang, J. Hu, W. Hua, M. Cheng, G. Wang and W. Fu, "Multiple 3-Phase PMA-SynRM With Delta Windings for Enhanced Fault Tolerance," in IEEE Transactions on Industrial Electronics, vol. 70, no. 2, pp. 1094-1104, Feb. 2023.

[17] M. Al-ani, A. Walker, G. Vakil, D. Gerada, C. Gerada and K. Paciura, "Modifications to PM-assisted Synchronous Reluctance Machine to Achieve Rare-Earth Free Heavy-duty Traction," in IEEE Journal of Emerging and Selected Topics in Power Electronics, 2022.

[18] A. Nobahari, A. Vahedi and R. Nasiri-Zarandi, "A Modified Permanent Magnet-Assisted Synchronous Reluctance Motor Design for Torque Characteristics Improvement," in IEEE Transactions on Energy Conversion, vol. 37, no. 2, pp. 989-998, June 2022.

[19] M. Degano et al., "Optimised Design of Permanent Magnet Assisted Synchronous Reluctance Machines for Household Appliances," in IEEE Transactions on Energy Conversion, vol. 36, no. 4, pp. 3084-3095, Dec. 2021.

[20] P. Kumar, Q. Ma, A. Al-Qarni, T. Chowdhury and A. El-Refaie, "Design Optimization and Comparison of PM-Assisted Synchronous Reluctance Machine using Different Magnet Combinations," 2022 IEEE Energy Conversion Congress and Exposition (ECCE), 2022, pp. 1-8.

[21] J. -C. Son and D. -K. Lim, "Optimal Design of PMa-SynRM for Electric Bicycle Traction Motor Using Adjustive-resolution Robustness Optimization Algorithm," 2022 IEEE 20th Biennial Conference on Electromagnetic Field Computation (CEFC), 2022, pp. 1-2.

[22] M. K. Islam, M. Karimi-Ghartemani and S. Choi, "Design of a Robust Optimal Controller for Five-Phase Permanent Magnet Assisted Synchronous Reluctance Motor in Electric Vehicle Application," 2021 IEEE Applied Power Electronics Conference and Exposition (APEC), 2021, pp. 1078-1085.

[23] M. Pastura, D. Barater, S. Nuzzo and G. Franceschini, "Multi Three-Phase Hairpin Windings for High-Speed Electrical Machine: Possible Implementations," 2021 IEEE Workshop on Electrical Machines Design, Control and Diagnosis (WEMDCD), 2021, pp. 113-118.

[24] Type sheets for industrial trucks, VDI Std. 2198, 2019.

[25] Energy efficiency of industrial trucks — Test methods — Part 1: General, ISO Standard 23308-1, 2020.

[26] Intelligent transport systems — Adaptive cruise control systems — Performance requirements and test procedures, ISO Standard 15622, 2018.

[27] K. Rana and D. C. Meena, "Self Excited Induction Generator for Isolated Pico Hydro Station in Remote Areas," 2018 2nd IEEE International Conference on Power Electronics, Intelligent Control and Energy Systems (ICPEICES), 2018, pp. 821-82